Sublinear and superlinear dependences of average charge and energy loss per ion on particle number for MeV/atom linear-chained carbon-cluster ions traversing a carbon foil

Toshiaki Kaneko

Department of Applied Physics, Okayama University of Science, 1-1 Ridai-cho, Kita-ku, Okayama-shi, Okayama, 700-0005, Japan

(Received 3 April 2012; published 16 July 2012)

The cluster effect in the average charge and the energy loss of swift carbon-cluster ions with kinetic energy of MeV per atom in a linear-chain structure with equal separation of 0.127 nm, passing through carbon foil, was theoretically investigated on the basis of the dielectric function formalism together with the wave-packet model. We assume that inside a foil the dissipated and the conservative forces due to electron polarization are acting on constituent partially stripped ions as well as the repulsive Coulomb forces. In addition, the reductive effect of the cluster average charge is incorporated in a self-consistent manner. On the other hand, outside a foil, only a repulsive Coulomb interaction is assumed to be working. The equation of motion for constituent ions is numerically solved using the molecular dynamics method under the action of the above forces. The calculated results are presented as a function of the incident orientation angle θ. By taking the average over θ, the energy loss per ion of the carbon cluster displays a sublinear dependence on the number of atoms at lower energies, while at higher energies it shows a superlinear dependence in spite of including the average charge reduction. These two trends in the energy loss are in good agreement with existing experimental results, in which not only the spatial correlation but also the reduction of cluster average charge is found to play a significant role.

DOI: 10.1103/PhysRevA.86.012901 PACS number(s): 34.50.Bw, 36.40.−c, 61.80.Lj

I. INTRODUCTION

Recently, cluster or polyatomic projectiles have attracted intensive interest in the field of investigating the interaction of high-energy cluster ions with solid materials from both the basic and applied viewpoints. For example, C_{60} fullerene ions and highly charged biomolecules have been accelerated at high energies (e.g., 10 MeV to 1 GeV) [1]. From the viewpoint of applications, cluster impact has the following advantages: one can (1) reduce the kinetic energy per atom at a given accelerated voltage, (2) suppress the charge-up effect in ion implantation, and (3) perform high-density particle irradiation in a narrow area. These properties are utilized in fabrication and processes, e.g., surface evaporation and surface etching by using a gas cluster ionized beam (GCIB) [2] with low kinetic energy (a few 10 eV per atom). From the basic physics viewpoint, on the other hand, the research subjects using polyatomic ion beams are widely ranging: fragmentation [3–5] and Coulomb explosion [6] of the clusters, multiple ionization [7], emissions of ions and neutrals [8], reduction of average charge [9–11], secondary electron emission [12–15], and energy deposition to a target [10,16–21], etc. In most cases, these subjects include an electron excitation process, which is correlated in space and time, induced by an ensemble of dense charged particles. This feature brings new results that are completely different from a single-ion penetration. In these excitation phenomena, the resultant effects induced per ion are sometimes stronger or weaker than those expected by single-ion incidence at an equivalent speed. Let us denote by $Y(n)$ a quantity per ion such as energy loss, average charge, the secondary electron yield, and so on, obtained under the impact of the cluster ion C_n^+, consisting of n atoms. In order to compare $Y(n)$ with the corresponding value $Y(1)$ under single-ion incidence, it is convenient to define $D \equiv Y(n) - Y(1)$ and $R \equiv Y(n)/Y(1)$. When $D > 0$ or $R > 1$, we call this the positive or the superlinear cluster effect, and in the opposite case we call it the negative or the sublinear cluster effect. Therefore, one recognizes that there will be a threshold of the cluster effect in the incidence energy. This threshold energy mainly depends on the number of constituent atoms, the spatial structure, the target element, and the penetration length of the foil. These features originate from a new character of the cluster ion beam, described by the number of constituent atoms and the spatial structure, in addition to the conventional character of the monoatomic ion beam, described by the ion speed, the ion element (or atomic number), and the distribution of the bound electrons.

The cluster effect has been found in the average charge [9–11], the energy-loss phenomena [10,16,18,21–23], and the secondary electron yield [12–15]. As for the average charge, Brunelle *et al.* [9] found at first a reduction of the cluster average charge per ion. Recently, Chiba *et al.* [11] reported the structure dependence of the cluster average charge using the Coulomb explosion imaging technique. They have extended this method to the divergence-angle measurement for various charge-state combinations [24]. Regarding the energy loss of a carbon cluster, the threshold energy exists around 1 MeV per atom. At incident energies larger than the threshold, the energy loss per ion, $\Delta E(n)$, displays the positive cluster effect, i.e., $D \equiv \Delta E(n) - \Delta E(1) > 0$ or $R \equiv \Delta E(n)/\Delta E(1) > 1$. In fact, this is experimentally supported by Baudin *et al.* [21] and also theoretically predicted [10]. On the other hand, there have been few data on the energy loss of carbon-cluster ions with the kinetic energy less than the threshold. In such a lower-energy region, we predicted that the cluster energy loss will show a negative effect [10]. As only one example, Brunelle *et al.* [18] experimentally obtained $D < 0$ for the 1.01 MeV/atom C_n^+ cluster ion penetrating a carbon foil. On the contrary, Heredia-Avalos *et al.* [22] insisted that the cluster effect was still positive in the corresponding case. Tomaschko *et al.* [23] reported that $D \simeq 0$ or $R \simeq 1$ for a rather thick (42 nm = 9.45 μg/cm^2) carbon target, although

with large error bars. As far as the author knows, there are few experimental data that obviously show the negative cluster effect in the energy loss for carbon incidence with the kinetic energy below the threshold. Recently, making use of a novel experimental method, Tomita *et al.* [25] clearly observed the negative cluster effect in the energy loss of the 0.5 MeV/atom carbon cluster C_n^+ ($n = 1-4$) penetrating a thin carbon foil. Under these situations, it is needed to clarify whether those effects could be predicted or not. To do so in a detailed manner, we included here the Coulomb explosion, the dissipated force, the polarization force, and the cluster average charge reduction in bulk. Thus, the aim of the paper is to show that the present detailed treatment predicts the negative cluster effect for the irradiation of carbon-cluster ions with lower (less than the threshold) kinetic energy and to show that it also leads to the positive cluster effect for clusters with the higher energies over the threshold. In Sec. II, the framework of the present analysis will be described. In Sec. III, numerical results and discussion will be given together with comparison with the existing data. Through this paper, m, e, and $\hbar$ denote, respectively, the electron rest mass, the elementary charge, and the Planck constant divided by 2π. In addition, the Bohr radius and the Bohr speed are denoted by $a_0 = \hbar^2/(me^2) = 0.529 \times 10^{-10}$ m and $v_0\ (= e^2/\hbar) = 2.19 \times 10^6$ m/s, respectively.

II. THEORETICAL MODEL

Here we describe the present theoretical model and quantities to evaluate the energy loss as well as average charge of a cluster moving in a solid, in order to elucidate the results and discussion clearly.

A. Cluster average charge

First we briefly describe the theory of the cluster average charge. The average charge of a single ion with atomic number Z moving in a foil at speed V is given in the fluid-mechanical picture by

$$\frac{Q}{Z} = \frac{2}{\sqrt{\pi}} \int_0^y dt \exp(-t^2), \quad y = \sqrt{\frac{3}{8}} \frac{V}{V_b}, \tag{1}$$

where $V_b = 1.045 Z^{2/3} v_0$ is the average speed of the electrons bound on the ion in a statistical model [10]. This expression was extended to cluster ions by modifying V_b by introducing the binding effect of surrounding ions via the potential energy. The resultant expression for the average charge Q_i of the ith ion in the cluster is given by

$$\frac{Q_i}{Z} = \frac{2}{\sqrt{\pi}} \int_0^y dt\ \exp(-t^2), \quad y = \sqrt{\frac{3}{8}} \frac{V}{V_{b,i}}, \tag{2}$$

with $V_{b,i} = [1.092 Z^{4/3} + \sum_{j(\neq i)} (2/m) V_{ji}(R_{ji})]^{\frac{1}{2}} v_0$. Here $V_{ji}(R_{ji})$ denotes the interaction potential energy per electron of the ith ion at $\vec{R}_i$ with the jth ion at $\vec{R}_j$. If $R_{ji} (= |\vec{R}_j - \vec{R}_i|)$ is large enough, $V_{ji}(R_{ji})$ reduces to the point-charge value $\frac{Q_j}{R_{ji}} e^2$. As a more general expression, we take in the Thomas-Fermi-Moliere (TFM) approximation the following expression:

$$V_{ji}(R) = \frac{Q_j e^2}{R} \left\{ 1 - \sum_{m=1}^{3} \alpha_m \exp\left(-\frac{\beta_m R}{\Lambda_i} \right) \right\} + \frac{N_j e^2}{R} \sum_{m=1}^{3} \sum_{\ell=1}^{3} \alpha_m \alpha_\ell \frac{\exp(-\beta_m R/\Lambda_i) - \exp(-\beta_\ell R/\Lambda_j)}{(\Lambda_i/\beta_m)^2 (\beta_\ell/\Lambda_j)^2 - 1}, \tag{3}$$

with $\Lambda_t = 0.6269 N_t^{2/3} a_0/(Z - N_t/7)$ and $N_t = Z - Q_t$ ($t = i, j$). In addition, we have $\alpha_1 = 0.10$, $\alpha_2 = 0.55$, $\alpha_3 = 0.35$, and $\beta_1 = 6.0$, $\beta_2 = 1.20$, $\beta_3 = 0.30$. It is well known that the average charge of a single ion moving in a material depends very weakly on the target material and it enables us to describe the charge well by only the ion speed and the atomic number. As for the cluster incidence, on the other hand, not only speeds of constituent ions but also the spatial structure of the cluster becomes important. At the same time, the average binding energy per electron reflects the structure-dependent effect of surrounding ions. The average charge of a given ion in the cluster depends on both the charges and the positions of other ions. I summarize that the surrounding ions strengthen the binding force of electrons and that the average charges of constituent ions have to be determined in a self-consistent manner.

B. Forces acting on individual ions

Let us assume that the cluster projectile moves in a target material with velocity $\vec{V}$, where the cluster is composed of homoatoms and contains n atoms of atomic number Z. We regard the cluster as an ensemble of partially stripped ions (PSIs), which are composed of a pointlike nucleus surrounded by the electron cloud. For convenience, the electron cloud of the jth ion is given by the TFM statistical distribution. Then the charge density of the jth ion located at the origin is given by

$$\rho_j(\vec{r}) = Z e\, \delta(\vec{r}) - e\rho_{je}(\vec{r}),$$
$$\rho_{je}(\vec{r}) = \frac{N_j}{4\pi r} \sum_{s=1}^{3} \alpha_s \left(\frac{\beta_s}{\Lambda_j} \right)^2 \exp\left(-\frac{\beta_s r}{\Lambda_j} \right). \tag{4}$$

Here N_j and Λ_j are the number of bound electrons and the size parameter of the electron cloud, respectively. The values of α_s, β_s ($s = 1,2,3$), and Λ_j are already given in the TFM distribution in Eq. (3). This function becomes infinite at $r = 0$ so that the statistical distribution of electrons in real space tend to be invalid near the nucleus. However, the form factor, i.e., the Fourier transform of the charge density in real space, derived from the above TFM distribution, is a rather nicely approximate function of that derived from the Hartree-Fock wave functions, in spite of its simple form.

Let us find the force $\vec{F}_j$ acting on the jth PSI, whose charge distribution is expressed by $\rho_j(\vec{r},t) = Ze\delta(\vec{r} - \vec{V}t) - e\rho_{je}(\vec{r} - \vec{V}t)$, moving at velocity $\vec{V}$ in a dielectric medium. Here the electric excitation is described by the dynamical dielectric function $\varepsilon(\vec{k},\omega)$. First we obtain the force due to

polarization as follows:

$$\vec{F}_j = -\int d^3r\, \rho_j(\vec{r},t)\nabla\varphi_{\rm ind}(\vec{r},t). \tag{5}$$

Here the induced scalar potential is decomposed using the induced charge density $\rho_{\rm ind}(\vec{k},\omega)$ in Fourier space as follows:

$$\varphi_{\rm ind}(\vec{r},t) = \frac{1}{(2\pi)^4}\int d^3k \int_{-\infty}^{+\infty} d\omega \frac{4\pi}{k^2}\rho_{\rm ind}(\vec{k},\omega) \times \exp\{i(\vec{k}\cdot\vec{r}-\omega t)\}. \tag{6}$$

The induced charge density is expressed by the dynamical dielectric function

$$\rho_{\rm ind}(\vec{k},\omega) = \left[\frac{1}{\varepsilon(\vec{k},\omega)} - 1\right]\rho_{\rm ext}(\vec{k},\omega). \tag{7}$$

The external charge density for the incident cluster ions in Fourier space is given by

$$\rho_{\rm ext}(\vec{k},\omega) = 2\pi\sum_s \rho_s(\vec{k})\exp(-i\vec{k}\cdot\vec{R}_s)\delta(\omega-\vec{k}\cdot\vec{V}), \tag{8}$$

where $\rho_s(\vec{k})$ denotes the charge density in Fourier space of the sth ion located at position vector $\vec{R}_s$ with respect to the center-of-mass (c.m.) of the cluster, moving at velocity $\vec{V}$ in a dielectric media. Here we assume the adiabatic condition under which the variation of speeds of constituent ions in the c.m. frame is much smaller than the c.m. speed of the cluster.

Under the above condition, we express the force acting on the jth ion in a simple form:

$$\vec{F}_j = -\frac{1}{2\pi^2}\int d^3k \int_{-\infty}^{+\omega} d\omega \frac{i\vec{k}}{k^2}\left[\frac{1}{\varepsilon(\vec{k},\omega)} - 1\right]\rho_j(-\vec{k}) \times \sum_s \rho_s(\vec{k})\exp(i\vec{k}\cdot\vec{R}_{js})\delta(\omega-\vec{k}\cdot\vec{V}), \tag{9}$$

with $\vec{R}_{js} = \vec{R}_j - \vec{R}_s$. In order to proceed further, the above force is decomposed in the perpendicular and the parallel components, $\vec{F}_{j\perp}$ and $\vec{F}_{jz}$, to the z direction of beam injection. After some algebra, we finally obtain

$$\vec{F}_j = \vec{F}_{j\perp} + \vec{F}_{jz}, \tag{10a}$$

$$\vec{F}_{j_\perp} = \frac{2}{\pi V}\int_0^\infty dk_\perp k_\perp^2 \int_0^\infty d\omega \rho_j(-\vec{k})\sum_s \rho_s(\vec{k}) \times \frac{J_1(k_\perp R_{js\perp})}{k_\perp^2 + (\omega/V)^2}\vec{n}_{js\perp}\left[\cos\left(\frac{\omega}{v}R_{jsz}\right)\mathrm{Re}\left\{\frac{1}{\varepsilon(k,\omega)} - 1\right\} - \sin\left(\frac{\omega}{v}R_{jsz}\right)\mathrm{Im}\left\{\frac{1}{\varepsilon(k,\omega)} - 1\right\}\right], \tag{10b}$$

$$\vec{F}_{j_z} = \frac{2}{\pi V^2}\int_0^\infty dk_\perp k_\perp \int_0^\infty d\omega\omega\rho_j(-\vec{k})\sum_s \rho_s(\vec{k}) \times \frac{J_0(k_\perp R_{js\perp})}{k_\perp^2 + (\omega/V)^2}\vec{n}_{jsz}\left[\cos\left(\frac{\omega}{v}R_{jsz}\right)\mathrm{Im}\left\{\frac{1}{\varepsilon(k,\omega)} - 1\right\} + \sin\left(\frac{\omega}{v}R_{jsz}\right)\mathrm{Re}\left\{\frac{1}{\varepsilon(k,\omega)} - 1\right\}\right], \tag{10c}$$

with $k^2 = k_\perp{}^2 + (\omega/V)^2$. Here $\vec{n}_{js\perp}$ and $\vec{n}_{jsz}$ are the unit vectors of the perpendicular and the parallel components of $\vec{R}_{js}$, respectively. The dielectric function $\varepsilon(k,\omega)$ for an electron gas at absolute zero temperature was given in an analytical form in [26]. Another dielectric function used here for describing excitation of the bound electrons was also derived [27]. The charge density $\rho_j(\vec{k})$ of the jth ion is given as $\rho_j(\vec{k}) = \{Z_j - \rho_{je}(\vec{k})\}e$, where $\rho_{je}(\vec{k})$, obtained from the Fourier transform of $\rho_{je}(\vec{r})$ in Eq. (4), includes the average number of the bound electrons, N_j, determined self-consistently by the ion speed V, the charges of surrounding ions, Q_j, and the spatial structure of the cluster. In Eqs. (10b) and (10c), $J_n(k_\perp R_{js\perp})(n = 0,1)$ denotes the n-th order Bessel function of the first kind. The subscripts z and $\perp$ of the arguments denote the components parallel and perpendicular to the incident ion beam, respectively. In addition, Re$\{a\}$ and Im$\{a\}$ are the real part and the imaginary part of a complex number a, respectively. It should be noted that there are two types of force involved in the expression of $\vec{F}_j$. One is the conservative force and the other is the dissipative force. The dissipative force can be discerned by absorption of energy, including the imaginary part of the dielectric function. On the other hand, the conservative force, including the real part of the dielectric function, does not absorb energy but satisfies the action-reaction law. In other words, action-reaction terms change sign when interchanging a variable $\vec{R}_j$ by a variable $\vec{R}_s$.

Another force is the Coulomb repulsive force acting among constituent ions, derived from the potential energy as follows:

$$\vec{F}_j = -\nabla_j V(\vec{R}_j),$$
$$V(\vec{R}) = \sum_{s(\neq j)}\int\int \frac{\rho_j(\vec{r}_1)\rho_s(\vec{r}_2)}{|\vec{R}+\vec{r}_1-\vec{r}_2|}d^3r_1 d^3r_2. \tag{11}$$

Here we remember that each ion is not a point charge but a partially stripped ion. One will see below that this is a general expression for a Coulomb interaction. In general, the scalar potential of an external charge is dynamically screened in the dielectric material. Let us start with a general expression for a force exerting on the jth ion, given by

$$\vec{F}_j = -\int d^3r\rho_j(\vec{r},t)\nabla\varphi_{\rm tot}(\vec{r},t). \tag{12}$$

Here the total scalar potential $\varphi_{\rm tot}(\vec{r},t)$ consists of the external potential $\varphi_{\rm ext}(\vec{r},t)$ plus the induced scalar potential $\varphi_{\rm ind}(\vec{r},t)$. In the Fourier space, we have

$$\varphi_{\rm tot}(\vec{k},\omega) = \varphi_{\rm ext}(\vec{k},\omega) + \varphi_{\rm ind}(\vec{k},\omega) = \frac{\varphi_{\rm ext}(\vec{k},\omega)}{\varepsilon(\vec{k},\omega)}, \tag{13}$$

and the scalar potentials in the real space are related with the corresponding charge densities in the Fourier space as follows:

$$\varphi_a(\vec{r},t) = \frac{1}{(2\pi)^4}\int d^3k\int_{-\infty}^{+\infty} d\omega\frac{4\pi}{k^2}\rho_a(\vec{k},\omega) \times \exp\{i(\vec{k}\cdot\vec{r}-\omega t)\}, \tag{14}$$

where the subscript represents $a =$ tot, ext, ind. The expression of the force in Eq. (12) includes the self-interaction terms so that, after removing them, we finally obtain the expression of the force $\vec{F}_j$, which consists of the Coulomb force and the expression of Eq. (10). As mentioned, there are

two contributions in Eq. (10), i.e., the dissipated (or friction) force and the conservative force. The conservative force and the Coulomb force result in the screened Coulomb force. Then we do not introduce the screened Coulomb force to describe a repulsive force but treat the unscreened Coulomb force separately.

It is interesting to describe the relation of the present forces and the conventional expression for the electronic stopping power of matter for the nonoriented cluster. It was done by averaging the force $\vec{F}_{jz}$ over the orientation of $\vec{R}_{ji}$. Let us denote by $\langle A\rangle$ the orientation average of a quantity A over $\vec{R}_{ji}$ keeping the magnitude R_{ji} constant. According to a mathematical formula, we have

$$\langle J_0(aR_\perp)\cos(bR_z)\rangle = \sin(R\sqrt{a^2+b^2})/(R\sqrt{a^2+b^2}), \tag{15a}$$

$$\langle J_0(aR_\perp)\sin(bR_z)\rangle = 0. \tag{15b}$$

Then we can finally obtain

$$\sum_j \langle F_{jz}\rangle = \frac{2}{\pi V^2}\int_0^{+\infty} dk\,\frac{1}{k}\langle|\rho_{\rm ext}(\vec{k})|^2\rangle \times \int_0^{kV} d\omega\omega\,{\rm Im}\left\{\frac{-1}{\varepsilon(k,\omega)}\right\}, \tag{16a}$$

$$\sum_j \langle \vec{F}_{j\perp}\rangle = \vec{0}, \tag{16b}$$

with

$$\langle|\rho_{\rm ext}(\vec{k})|^2\rangle = \sum_j [\rho_j(k)]^2 + \sum_j\sum_{\ell(\neq j)} \rho_j(k)\,\rho_\ell(k)\frac{\sin(kR_{j\ell})}{kR_{j\ell}}. \tag{16c}$$

Here $R_{j\ell} = |\vec{R}_j - \vec{R}_\ell|$ is the relative distance between the jth and ℓth ions. Equation (16a) is the familiar expression of the electronic stopping power for a nonoriented cluster projectile, whose charge density in Fourier space is given by Eq. (16c). It is quite natural that the perpendicular component of the force vanishes. From the above derivation, we confirm that Eq. (10) is a general expression of the forces in a dielectric medium, including the conservative and the dissipative ones as well as the dynamic screened effect.

C. Enlargement of the internuclear separation due to elastic collision

In this section, we present the contribution of elastic collisions between a single ion and a target atom in the small-angle approximation. As an ion traverses a solid, it experiences subsequent elastic scatterings, and as a result, the moving ion has an angular distribution around the incident direction [28–31]. Here we consider the effect of this phenomenon on enlargement of the internuclear distance. For simplicity, we approximately describe the angular distribution by a Gaussian $f(\theta) = A\exp(-\theta^2/\langle\theta^2\rangle)$ as a function of deflection angle θ with the normalization constant A. This angular distribution gives rise to a lateral spread of the ion position perpendicular to the incident direction. Let us assume the lateral spread $\vec{s}$ of the ion due to elastic scattering is also described by a Gaussian $f(\vec{s}) = \frac{1}{\pi\,\Delta_1^2}\exp\{-(\vec{s}-\vec{s}_0)^2/\Delta_1^2\}$, where $\vec{s}_0$ is the lateral position without elastic scattering. Here we introduce the lateral spreading parameter Δ_1^2, which is related to the angular distribution parameter as below. First, using this expression, we estimate the change of internuclear separation of two independent ions located at positions $\vec{r}_1 = (\vec{s}_1, z_1)$ and $\vec{r}_2 = (\vec{s}_2, z_2)$, due to one elastic collision. This can be done by taking the following average: $\langle|\vec{r}_1 - \vec{r}_2|^2\rangle = |z_1 - z_2|^2 + \langle|\vec{s}_1 - \vec{s}_2|^2\rangle$, where

$$\langle|\vec{s}_1 - \vec{s}_2|^2\rangle = \int d^2s_1 \int d^2s_2 |\vec{s}_1 - \vec{s}_2|^2 f(\vec{s}_1) f(\vec{s}_2) = |\vec{s_{10}} - \vec{s_{20}}|^2 + 2\Delta_1^2. \tag{17}$$

As a consequence, the interionic separation without elastic collision, $d_{12} = |\vec{r}_1 - \vec{r}_2|$, is enlarged up to $\widetilde{d_{12}} = (d_{12}^2 + 2\Delta_1^2)^{1/2}$ by one elastic collision. Next we relate this expression to the cross section σ of a single elastic scattering. As the mean free path λ of a single elastic scattering is given by $\lambda = (N\sigma)^{-1}$, so that the number n of elastic collisions during the passage is given by $n = \tau/\lambda = N\sigma\tau$, where τ is the total path length or the foil thickness. If we take into account the relation of $\theta_{\rm L} = \frac{1}{2}\theta_{\rm c.m.}$ between the scattering angle $\theta_{\rm L}$ in the laboratory (L) system and $\theta_{\rm c.m.}$ in the c.m. system, the lateral spreading due to a single scattering amounts to $\Delta_1^2 = \lambda^2\langle\theta^2\rangle_L = \lambda^2\frac{1}{4}\langle\theta^2\rangle_{\rm c.m.}$, and the total lateral spreading amounts to $\Delta_{\rm total}^2 = 2n\Delta_1^2$ in the case of $\lambda < \tau$. Here we define $\langle\theta^2\rangle_{\rm c.m.} = \int d\Omega\theta^2\frac{d\sigma}{d\Omega}/\sigma$ using a differential elastic scattering cross section $\frac{d\sigma}{d\Omega}$. When the TFM potential is employed for a two-body scattering, one obtains the differential scattering cross section in the c.m. system as

$$\frac{d\sigma}{d\Omega} = \left(\frac{Z_1Z_2e^2}{4E}\right)^2\left[\sum_{j=1}^{3}\frac{\alpha_j}{\sin^2(\theta/2) + (\beta_j/2k_0a)^2}\right]^2$$

in Born approximation, where $E = (\hbar k_0)^2/(2\mu)$, $k_0 = \mu V/\hbar$, $\mu = M_1M_2/(M_1+M_2)$, and $a = 0.8853a_0\left(Z_1^{1/2} + Z_2^{1/2}\right)^{-2/3}$. The values of α_j, β_j (j = 1–3) are given in Eq. (3). Up to here, we evaluate the contribution of the lateral spreading with use of a statistical potential. We show that small-angle elastic collisions have an effect of enlargement of the internuclear separation through the lateral broadening.

D. Energy straggling and postfoil interaction

It is well known that the energy loss of swift particles transiting a material fluctuates around its average value, resulting in spreading energy spectrum. This fluctuation, called the energy straggling, has several causes: statistical fluctuations in the energy transfer to electrons [32], nonuniformity of thickness of a target foil, molecular target effect [33], and fluctuation of charge state via electron-capture and -loss processes [34]. Among them, the dominant contribution originates from collisions with the target electrons in the bulk, which of a

partially stripped jth ion is given in the dielectric form as

$$\Omega_j^2/(Nx) = \frac{2\hbar}{\pi V^2}\int_0^{+\infty} dk\frac{1}{k}|\rho_j(\vec{k})|^2 \times \int_0^{kV} d\omega\omega^2 \mathrm{Im}\left\{\frac{-1}{\varepsilon(k,\omega)}\right\}, \quad (18)$$

where N and x denote the number density of target atoms and the penetration path length.

Here we present another contribution which is unique to cluster impact. It comes from the postfoil Coulomb interaction. In order to see clearly, we assume a cluster composed of two particles with masses m_1 and m_2. Emerging from a foil, their charges and velocities are assumed q_1, $\vec{v}_1$ and q_2, $\vec{v}_2$, respectively. The velocity of the c.m. is given by $\vec{V}_G = \frac{m_1\vec{v}_1+m_2\vec{v}_2}{m_1+m_2}$, and the relative velocities in the c.m. frame are $\vec{u}_1 = \vec{v}_1 - \vec{V}_G$ and $\vec{u}_2 = \vec{v}_2 - \vec{V}_G$. Consequently, the energy conservation law in the c.m. frame yields $\frac{1}{2}m_1u_1^2 + \frac{1}{2}m_2u_2^2 + \frac{q_1q_2}{R_0} = \frac{1}{2}m_1u_{1\infty}^2 + \frac{1}{2}m_2u_{2\infty}^2$. Here R_0 indicates the relative distance between two particles when exiting a foil, and $u_{1\infty}$ and $u_{2\infty}$ denote the final speeds of particles 1 and 2 when infinitely far apart from each other. With use of the momentum conservation law, one can determine $u_{1\infty}$ and $u_{2\infty}$. The average energy in the laboratory (L) frame under the action of Coulomb explosion is given by $E_{av} = \frac{1}{2}(\frac{1}{2}m_1v_{1\infty}^2 + \frac{1}{2}m_2v_{2\infty}^2)$, so that the fluctuation of energy is evaluated as $\Delta\Omega = |E_{av} - \frac{1}{2}m_1v_{1\infty}^2| = |E_{av} - \frac{1}{2}m_2v_{2\infty}^2|$. This expression finally becomes

$$\Delta\Omega = \frac{1}{4}|(m_2-m_1)V_G^2 + m_2u_{2\infty}^2 - m_1u_{1\infty}^2 - 2(m_2u_{2\infty} + m_1u_{1\infty})\vec{V}_G\cdot\vec{e}|,$$

where $\vec{e}$ is the unit vector representing the direction of Coulomb explosion. In the special case of homoatom clusters ($m_1 = m_2 = m$), this reduces to

$$\Delta\Omega = \frac{1}{4}m\left|v_1^2 - v_2^2\right|\sqrt{1 + \frac{4}{(\vec{v}_1-\vec{v}_2)^2}\frac{q_1q_2}{mR_0}}. \quad (19)$$

If we neglect the postfoil interaction, it is easily found that the fluctuation of energy is given by $\Delta\Omega_0 = |\frac{1}{2}(\frac{mv_1^2}{2} + \frac{mv_2^2}{2}) - \frac{mv_1^2}{2}| = \frac{1}{4}m|v_1^2 - v_2^2|$. Thus the Coulomb potential energy is converted to the kinetic energy of emerging ions in a way that enlarges the difference in the kinetic energy. This role is played similarly for more complicated clusters coming out from a foil target. Finally, I would like to stress that the energy straggling due to the postfoil interaction is a unique process to cluster impact, where the average (or the whole) energy loss of a cluster could not be influenced as long as all constituent ions are detected after penetrating a foil.

III. NUMERICAL RESULTS AND DISCUSSION

We treated the carbon clusters C_n^+ (n = 1–6) in a linear-chain structure with equal spacing of $2.4a_0 = 0.127$ nm, normally incident on a thin carbon target. The incident kinetic energy ranges from 0.5 to 5 MeV/atom. Here the incidence of the cluster is axially symmetric with respect to the incident direction so that it is characterized by the polar angle θ between the cluster axis and the direction of incident velocity and also it is independent of the azimuth angle. In our calculation, the scenario is the following: The cluster is injected with a given polar angle. On entrance, each ion becomes a PSI with an average number of bound electrons that is determined by the cluster average charge theory. Inside the target, the individual ions are governed by the Coulomb force and the polarization force. We solve the equation of motion of the constituent ions in the cluster using the molecular dynamics (MD) method. On emergence from the target foil, the Coulomb interaction works only among the partially stripped ions, where individual ions are assumed to keep the average charge, determined in the bulk target. Therefore, the edge effect or the surface effect is not taken into account. This is valid because the interaction time between the surface and the ions penetrating a foil is very small in our case. Thus the present situation is completely different from that of grazing incidence.

It is well known that the dielectric function of the electron gas includes two excitation modes. One is the single-electron excitation and the other is the plasmon (or collective) excitation. For the former, we use the analytical expression derived by Lindhard [25], where four outer-shell electrons per carbon atom are assumed to participate in the electron gas. This assumption leads to a bulk plasmon energy $\hbar\omega_p = 25$ eV for a carbon target. For the latter, we adopt the following expression in the high-frequency limit, including the damping effect as $1/\varepsilon = 1 + \omega_p^2/(\omega^2 - \omega_p^2 + i\omega\gamma)$, where the damping constant relating to the lifetime of a plasmon is set to $\hbar\gamma = 3.3$ eV. In addition, the excitation of two inner-shell electrons is taken into account in the dielectric formalism [27].

First, let us consider the lower-incident-energy case. In Fig. 1, we show the average charge $Q(1)$ and the kinetic energy $E(1)$ in units of keV of a single carbon ion incident at kinetic energy of 0.5 MeV/atom on a carbon target, as a function of penetration depth in units of the Bohr radius a_0. Here, the charge state of the ion is assumed to attain to an equilibrium state as soon as it enters the target. This will be valid because the depth during which the charge state is in a preequilibrium state is very thin (e.g., $20a_0$). For a single-ion incidence, only the friction force works so that the ion loses its kinetic energy at the rate of the stopping power as it penetrates the target more deeply. Also the average charge, depending on the speed of the ion, is decreasing with decreasing speed. The values of the kinetic energy and the average charge as a function of the penetration depth are standard, since the corresponding quantities per ion for the cluster incidence will be compared with those for the single-ion incidence at equivalent speeds. An example of a higher-energy case (2 MeV/atom) was already shown in Ref. [10].

Let us move on to the cluster incidence. We define the θ-dependent energy loss and average charge per ion for a C_n^+ incidence, respectively, by $\Delta E(n,\theta) = (1/n)\sum_{j=1}^n dE_j$ and $Q(n,\theta) = (1/n)\sum_{j=1}^n Q_j$ with $dE_j = E_0 - E_j$. Here E_0 denotes the kinetic energy per atom of the incident cluster, and E_j and Q_j denote, respectively, the kinetic energy and the average charge of the jth constituent ion, far enough away from the target foil. We calculated step by step the kinetic energies and the average charges with use of MD calculation and finally obtained E_j's and Q_j's for individual ions, which

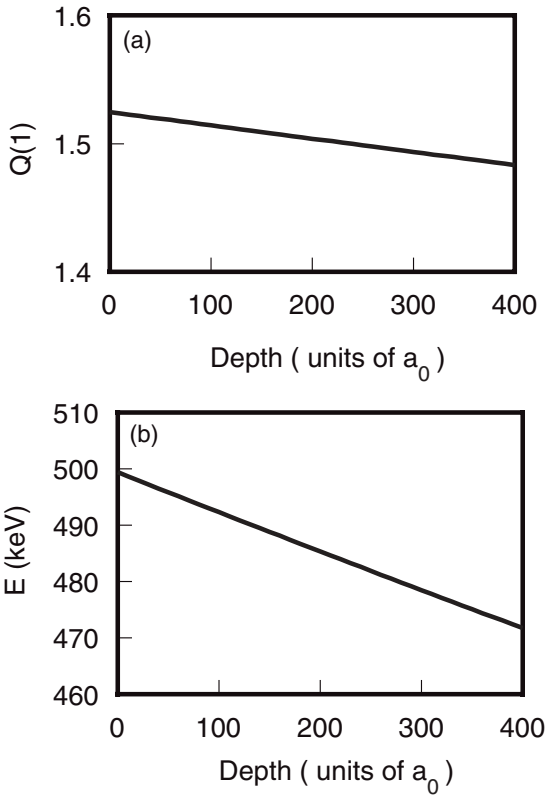

FIG. 1. (a) The average charge $Q(1)$ and (b) the kinetic energy E in units of keV of a carbon ion incident at 0.50 MeV/atom on a carbon target, calculated as a function of penetration depth in units of a_0.

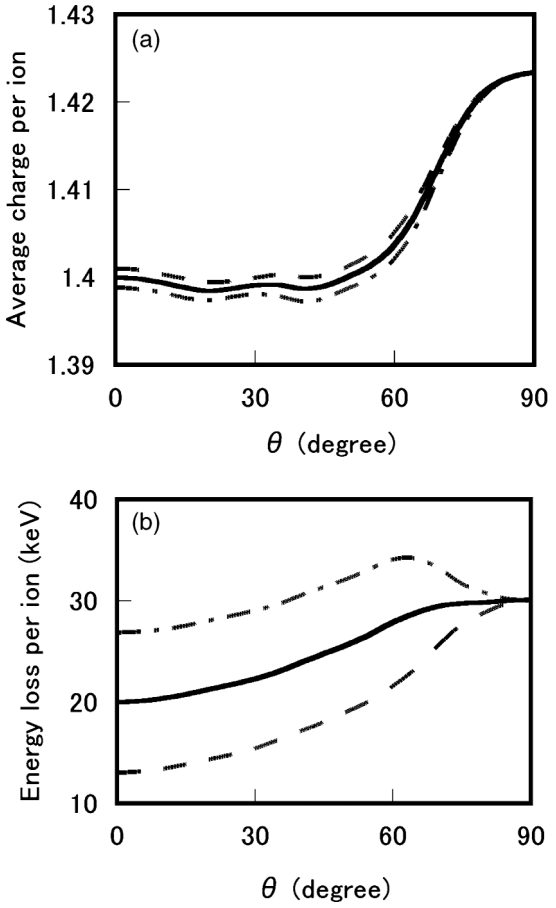

FIG. 2. (a) Average charges and (b) the energy losses per ion (in units of keV) of constituent ions penetrating a carbon target of $400a_0$ thickness, calculated for a 0.50 MeV/atom C_2^+ cluster incidence as a function of angle θ: the dashed lines represent the leading ion and the dash-dot lines the trailing ion. The solid lines indicate (a) $Q(2,\theta)$ and (b) $\Delta E(2,\theta)$.

depend on the incident polar angle θ. Here, $\theta = 0^\circ$ ($\theta = 90^\circ$) means that the cluster axis, or the alignment direction of atoms, is parallel (perpendicular) to the incident direction.

Figure 2 shows the average charge and the average energy loss of constituent ions as a function of θ for 0.5 MeV/atom C_2^+ cluster ions passing through a carbon foil of $400a_0$ thickness. In Fig. 2(a), the dashed line and the dash-dot line indicate the average charges Q_1 and Q_2, of the leading and the trailing ions, respectively, and the solid line indicates the average value $Q(2,\theta)$. From this figure, the average charges of the two constituent ions are almost the same value up to about $\theta = 60^\circ$, while beyond that angle the average charges gradually increase a bit to the maximum value at $\theta = 90^\circ$. This is due to the enlargement of the interatomic separation and the spatial symmetry at the exit surface. According to the cluster average charge theory [10], the average charges at infinite separation converge to the corresponding value of the single ion with the equivalent speed. Then the relation of $Q(2,\theta = 90^\circ) < Q_1 = 1.483$ means that the interatomic separation at the exit surface is not as large as the influence of other ions is negligible. Figure 2(b) shows the energy losses of the leading ion and the trailing ion, indicated by the dashed line and the dash-dot line, respectively. The average energy loss per ion $\Delta E(2,\theta)$ is indicated by the solid line. In the small-θ region, the leading ion loses its kinetic energy less than the trailing ion. This is caused by the postfoil Coulomb interaction, through which the leading ion is pushed forward and the trailing ion is pulled backward so that the difference in their kinetic energies becomes enlarged. At $\theta = 90^\circ$ in Fig. 2(b), however, they have the same kinetic energy. This result is reasonable since the two ions are symmetric in space and in equivalent positions. It is interesting that the energy difference of about 14 keV obtained for $\theta > 60^\circ$ becomes smaller with increasing θ and at last vanishes at $\theta = 90^\circ$. The average energy loss per ion $\Delta E(2,\theta)$ is a monotonically increasing function of θ from a minimum at $\theta = 0$ to a maximum at $\theta = 90^\circ$. It means that the energy loss of an aligned ($\theta = 0$) diatomic molecular ion is less than that of a randomly oriented one. This situation agrees with the results obtained for the incidence of other diatomic ions with an aligned interatomic axis [35,36].

Figure 3 shows the average charge and the average energy loss of constituent ions for the 0.5 MeV/atom C_3^+ cluster incidence, and is similar to Fig. 2. The average charges of the leading, the central, and the trailing ions in Fig. 3(a) are represented by the dashed line, the dash-dot-dot line, and the dash-dot line, respectively. The solid line displays the average charge $Q(3,\theta)$. At a glance, they tend to increase gradually with respect to θ as seen for C_2^+ in Fig. 2. Compared with the central ion, the average charges of the two edge ions are relatively large and equal at $\theta = 90^\circ$. The average charge of the central ion is always smaller than those of the edge ions. This

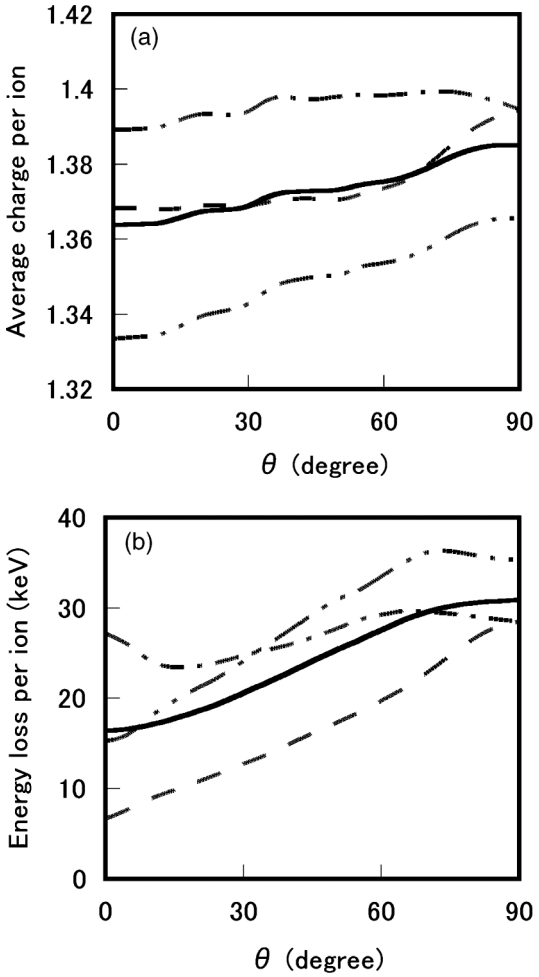

FIG. 3. (a) Average charges and (b) the energy losses per ion (in units of keV) of constituent ions penetrating a carbon target of $400a_0$ thickness, calculated for a 0.50 MeV/atom C_3^+ cluster incidence as a function of angle θ: the dashed lines represent the leading ion, the dash-dot-dot lines the central ion, and the dash-dot lines the trailing ion. The solid lines indicate (a) $Q(3,\theta)$ and (b) $\Delta E(3,\theta)$.

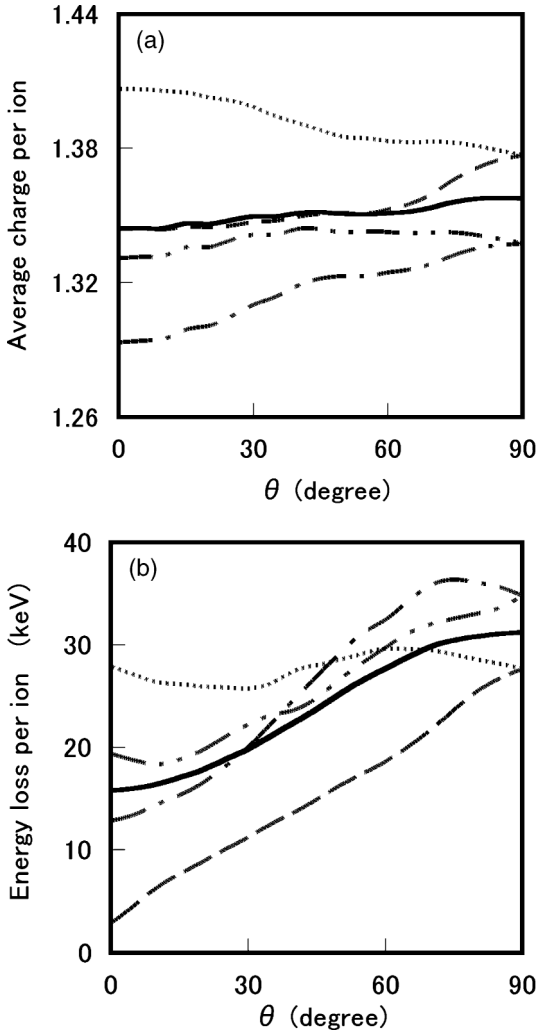

FIG. 4. (a) Average charges and (b) the energy losses per ion (in units of keV) of constituent ions penetrating a carbon target of $400a_0$ thickness, calculated for a 0.50 MeV/atom C_4^+ cluster incidence as a function of angle θ: the dashed lines represent the leading ion, the dash-dot lines the second ion, the dash-dot-dot lines the third ion, and the dotted lines the trailing ion. The solid lines indicate (a) $Q(4,\theta)$ and (b) $\Delta E(4,\theta)$.

feature comes from the magnitude of the binding energy, as is first predicted by the cluster average charge theory [10] with Coulomb repulsive force and without the polarization force. Now Fig. 3(a) also shows that this remarkable feature in the cluster average charge is still valid even if the polarization force is taken into account, and it is also consistent with the first experimental observation by Chiba *et al.* [11] with use of the 1 MeV/atom C_3^+ cluster. Figure 3(b) shows the energy losses of the leading, the central, and the trailing ions, drawn by the dashed line, the dash-dot-dot line, and the dash-dot line, respectively. The solid line indicates the average energy loss per ion $\Delta E(3,\theta)$. At $\theta = 0$, the magnitude of the energy loss is in order of the trailing, the central, and the leading ions, while at $\theta = 90^\circ$, the energy loss of the central ion is the largest and those of the two edge ions are equal. $\Delta E(3,\theta)$ is monotonically increasing with increasing θ from a minimum value at $\theta = 0$; there is also the same feature in the C_2^+ incidence.

Figure 4 shows the average charge and the average energy loss of constituent ions for the 0.5 MeV/atom C_4^+ cluster incidence on a carbon foil of $400a_0$ thickness. In Fig. 4(a), the average charges of the leading, the second, the third, and the trailing ions are represented by the dashed line, the dash-dot line, the dash-dot-dot line, and the dotted line, respectively. The solid line displays the average charge $Q(4,\theta)$. The difference in the average charges of individual ions is relatively large at $\theta = 0$, but it becomes smaller at $\theta = 90^\circ$. In this cluster the average charges of the two edge ions are larger than those of the two inner ions, due to the spatial symmetry and the magnitude of the binding force. At a glance, the θ-dependent variation of $Q(4,\theta)$ is weaker than those of $Q(2,\theta)$ and $Q(3,\theta)$. Figure 4(b) represents the energy losses of constituent ions. At $\theta = 0$, the leading, the second, the third, and the trailing ions have the energy loss in magnitude in this order. On the other hand, at $\theta = 90^\circ$ the two edge ions have the energy losses larger than those of the two inner ions. This means that the two inner ions are behind the two edge ions and the linear-chain structure at the entrance changes to a bent one at the exit of the foil

as is also seen in a C_3^+ penetration. The energy loss per ion $\Delta E(4,\theta)$ is also an increasing function of θ, as is the same in the C_2^+ and C_3^+ clusters. Regarding heavier clusters, $Q(n,\theta)$ and $\Delta E(n,\theta)$ for C_n^+ ($n = 5,6$) have a similar character of the θ dependences to those for smaller clusters C_n^+ ($n = 2$–4).

As a short summary, for a relatively low-MeV/atom cluster, the value of $Q(n,\theta)$ tends to increase with the increasing θ for smaller clusters, while the variation of $Q(n,\theta)$ with respect to θ becomes weaker for larger clusters. From this tendency, we may conjecture that the increase of the number of ions smears out the variation of $Q(n,\theta)$. In other words, it leads to the idea that the influence of surrounding ions may be mainly limited to the nearest- or the next-nearest-neighbor ions, and consequently the edge ions play a tiny role in the average charge for clusters consisting of a lot of atoms.

Let us move on to the orientation-averaged quantities, derived from the θ-dependent quantities. In general, the θ-dependent quantity $Y(n,\theta)$ obtained for the incidence of the cluster C_n^+ in a linear-chain structure leads to the averaged value over the allowed θ values by taking into account the weight function $W(\theta) = \sin\theta$ for axial symmetry. Thus we obtain the average value per ion, $Y(n)$, from the following definition:

$$Y(n) = \int_0^{\pi/2} d\theta W(\theta) Y(n,\theta) \Big/ \int_0^{\pi/2} d\theta W(\theta) = \int_0^{\pi/2} d\theta \sin\theta Y(n,\theta). \quad (20)$$

On the basis of the above consideration, the average charge per ion, $Q(n)$, and the average energy loss per ion, $\Delta E(n)$, calculated for the 0.50 MeV/atom C_n^+ cluster incident on a carbon foil of $400a_0$ thickness are shown as the solid squares in Fig. 5. There one finds that $Q(n)$ in Fig. 5(a) decreases with increasing number n of constituent atoms in the cluster, and that in the case of $n = 6$, it is reduced more than 10%, compared with $Q(1)$ for a single carbon atom with an equivalent speed. On the other hand, $\Delta E(n)$ in Fig. 5(b) tends to gradually decrease to $n = 3$ and saturate in a range of $n = 3$–6. In addition, the reduction of the relative energy loss per ion, $\Delta E(n)/\Delta E(1)$, amounts to 5% at most, representing a significant contrast to the average charge reduction. These two remarks mean that both the average charge and the energy loss per ion for the clusters depend on the number of constituent atoms weaker than the linear relation. Recently, Tomita *et al.* [24] measured the energy loss of the constituent ions for carbon clusters C_n^+ ($n = 1$–4) with kinetic energy 0.50 MeV/atom, penetrating a carbon foil of thickness 5.7 μg/cm^2. Their results lead to $\Delta E(n)/\Delta E(1) \approx 0.95$, which is in good agreement with the calculated result shown in Fig. 5. In order to confirm to what extent the average charge reduction contributes, we also carried out the similar calculation for a carbon foil of $480a_0$ thickness with and without taking into account the cluster average charge reduction. The calculated result without charge reduction is drawn by solid triangles in Fig. 5(b) for the clusters C_n^+ ($n = 2$–4), which shows that the energy loss per ion amounts to a few percent reduction. On the other hand, the results with charge reduction included are plotted as the open circles, which are close to the values for a carbon foil of $400a_0$ thickness. This means that the reduction

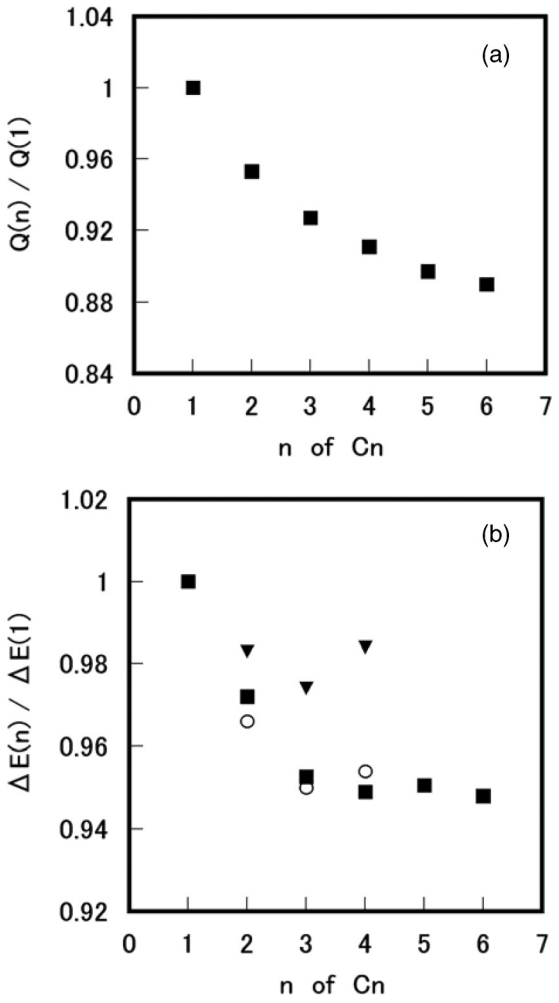

FIG. 5. The n dependences of (a) the ratio of the average charge per ion $Q(n)/Q(1)$ and (b) the ratio of the energy loss per ion, $\Delta E(n)/\Delta E(1)$, calculated for the 0.50 MeV/atom C_n^+ ($n = 1$–6) incidence on carbon target of thickness d. Solid squares are for $d = 400a_0$ with reduction of the cluster average charge; the open circles are for $d = 480a_0$ with reduction of the cluster average charge; and the solid triangles are for $d = 480a_0$ without reduction of the cluster average charge.

value is suppressed to be about half in the corresponding cases where the charge reduction effect is excluded.

In the above cases, we concentrate on the emergence of the sublinear (or negative) cluster effect in detail at relatively lower energy (i.e., 0.5 MeV/atom), and we confirm the existence of the sublinear effect. Next, in order to look into implementation of the present theory, we consider the higher-incident-energy cases, where the superlinear (or the positive) cluster effect will be expected. Figure 6 shows the average charge per ion $Q(n,\theta)$ for a C_n ($n = 2$–6) cluster ion penetrating a carbon foil of $480a_0$ thickness at $E = 4.8$ MeV/atom. One sees in Fig. 6(a) that $Q(n,\theta)$ is almost constant, representing a very weak θ dependence. Moreover, with increasing number of atoms, the average charge is decreasing. This latter tendency is also valid at the lower energies. Figure 6(b) represents a remarkable feature in $\Delta E(n,\theta)$. At $E = 4.80$ MeV/atom, $\Delta E(n,\theta)$ has a maximum around $\theta = 35^\circ$–40°, and $\Delta E(n,\theta)$ at lower

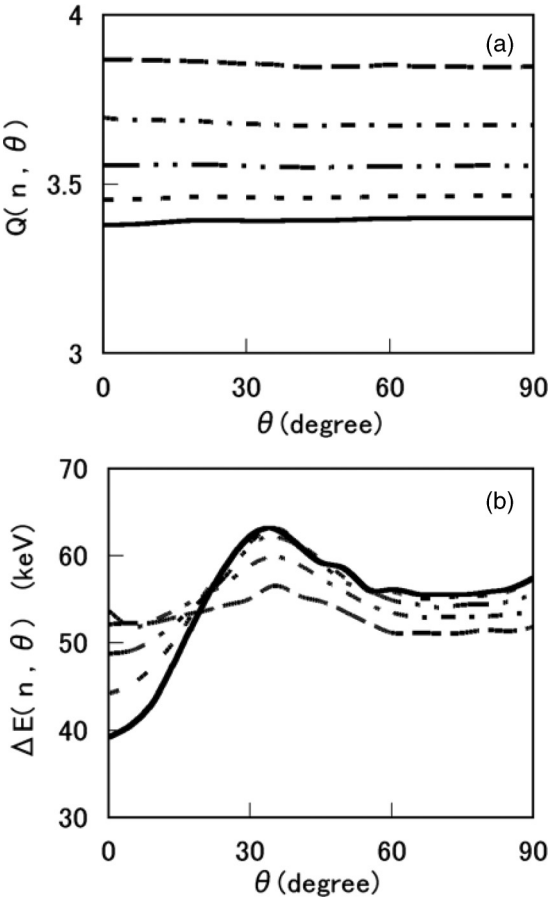

FIG. 6. (a) $Q(n,\theta)$ and (b) $\Delta E(n,\theta)$ for a C_n^+ ($n = 1$–6) at 4.8 MeV/atom, calculated as a function of incident orientation angle θ: $n = 2$ (dashed lines), $n = 3$ (dash-dot lines), $n = 4$ (dash-dot-dot lines), $n = 5$ (dotted lines), and $n = 6$ (solid lines).

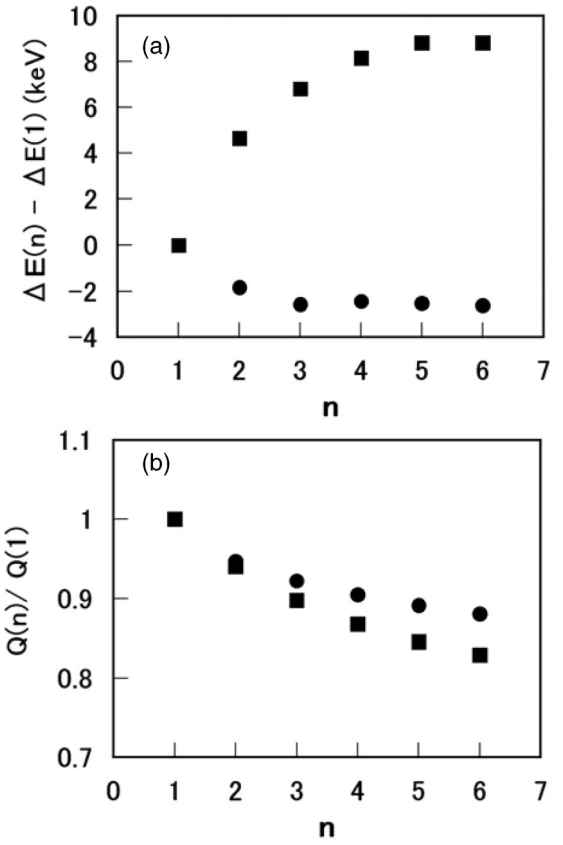

FIG. 7. (a) $\Delta E(n) - \Delta E(1)$ vs n, and (b) $Q(n)/Q(1)$ vs n, calculated for a C_n ($n = 2$–6) at the incident energy of 4.8 MeV/atom (solid squares) and 675 keV/atom (solid circles).

θ decreases with increasing n. On the contrary, at $E = 500$ keV/atom as shown in Figs. 2(b), 3(b), and 4(b), $\Delta E(n,\theta)$ ($n = 2$–4) monotonically increases with increasing θ, and the perpendicular orientation ($\theta = 90^\circ$) yields the maximum value of the average energy loss. Moreover, in Fig. 6(b), $\Delta E(n,0)$ decreases and $\Delta E(n,90)$ increases with increasing n. Namely, they display an opposite trend, and the difference between them, i.e., $\Delta E(n,90) - \Delta E(n,0)$, becomes larger for larger n. The increase of $\Delta E(n,\theta)$ around $\theta = 90^\circ$ is found at both $E = 4.8$ MeV/atom and 500 keV/atom. Thus, one recognizes that the n and θ dependences of $\Delta E(n,\theta)$ display characteristic features, depending on the incident energy. These tendencies are due to the force originating from the electron polarization. At low incident energies, the induced electronic polarization potential contributes to the static screening of the electric fields of the ion; however, at relatively high incident energies, it could not accompany the moving ion so that it tends to oscillate and becomes strong, because of the higher average charge. This complex behavior influences the motion of constituent ions, and is different from the monotonic effect of a Coulomb repulsion potential. Finally, the difference in $\Delta E(n,\theta)$ at $E = 4.8$ MeV/atom between the maximum and the minimum of $\Delta E(n,\theta)$ increases from 5 keV for C_2^+ to 24 keV for C_6^+. It is noticed that in case of $n = 2$, the difference between the maximum and the minimum values at $E = 4.8$ MeV/atom is smaller than that obtained at $E = 500$ keV/atom. Thus, inclusion of the polarization force brings a different aspect, depending on the incident energy.

Hereafter we present the θ-averaged energy loss per ion $\Delta E(n)$ and the θ-averaged average charge per ion $Q(n)$. Figure 7(a) shows the difference of the energy loss per ion, $\Delta E(n) - \Delta E(1)$ for a C_n^+ ion penetrating a carbon foil of $480a_0$ thickness, as a function of the particle number n, where the positive cluster effect is found at $E = 4.8$ MeV/atom and the negative one is seen at $E = 675$ keV/atom. In the lower-energy case, the negative effect in $\Delta E(n) - \Delta E(1)$ seems to saturate at $n = 3$, while the positive effect does so at $n = 5$. On the other hand, the average charge ratio $Q(n)/Q(1)$ in Fig. 7(b) shows the negative effect in both cases of $E = 4.8$ MeV/atom and $E = 675$ keV/atom, and the degree of suppression is stronger at $E = 4.8$ MeV/atom. This is because the dwell time in a foil is shorter and expansion of mutual separation among ions is not evolved so much, which results in a stronger influence of the surrounding ions.

Finally, in order to confirm the cluster effect in both energy loss and average charge in a wide energy range, we present $Q(n)/Q(1)$ in Fig. 8 and $\Delta E(n) - \Delta E(1)$ in Fig. 10 in the incident energy range from 0.30 MeV/atom to ~5 or 6 MeV/atom for a C_n^+ ($n = 2,4,6$) penetrating a carbon foil together with the existing experimental data. In our calculation, the foil thickness is set to be $480a_0$ (~25.4 nm), or, 5.72 μg/cm^2. Figure 8 indicates that the calculated average charge ratio decreases with increasing both the incident energy

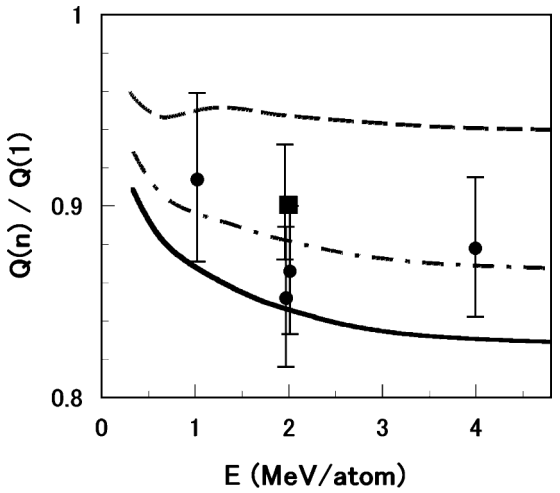

FIG. 8. $Q(n)/Q(1)$ calculated as a function of the incident energy for a C_n ($n = 2,4,6$) penetrating carbon foil of $480a_0$ (=5.7 μg/cm^2) thickness ($n = 2$, dashed line; $n = 4$, dash-dot line; and $n = 6$, solid line), together with the experimental data [9] for 5.30 μg/cm^2 carbon foil ($n = 3$, ■; $n = 5$, ●).

and the number of constituent ions, except for a very small dip appearing in the C_2 case. In the case of C_6 incidence, the value of $Q(n)/Q(1)$ is reduced to about 0.83. For reference, the experimental data, obtained by Brunelle *et al.* [9] for C_3^+ and C_5^+ ions penetrating a carbon foil of 5.30 μg/cm^2, are plotted by the solid squares and the solid circles, respectively. Though they have large error bars, the data around $E = 2$ MeV/atom show that a larger cluster has a lower average charge ratio. The decreasing dependence of the calculated charge ratio on the particle number, which is seen up to 4.8 MeV/atom (i.e., $v = 4v_0$), is supported by the existing data. However, one might be aware that the average charge ratio has to approach unity at extremely high speed. In order to confirm it, we present Fig. 9, where the calculated values of $Q(n)$ ($n = 2,4,6$) for a linear-chained C_n with equal interionic separation of $2.4a_0$, are drawn in a wider range of speed v in units of v_0, together with $Q(1)$. One finds that the dashed line ($n = 2$), the dot-dash line

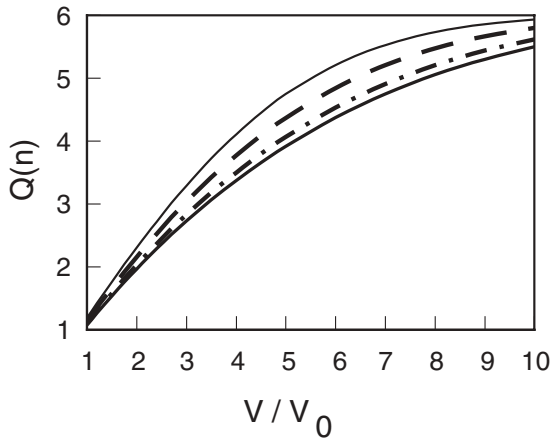

FIG. 9. $Q(n)$ calculated for C_n ($n = 2,4,6$) with equal interionic separation of $2.4a_0$, together with $Q(1)$ (thin solid line) as a function of speed v in units of v_0 ($n = 2$, dashed line; $n = 4$, dot-dash line; and $n = 6$, thick solid line).

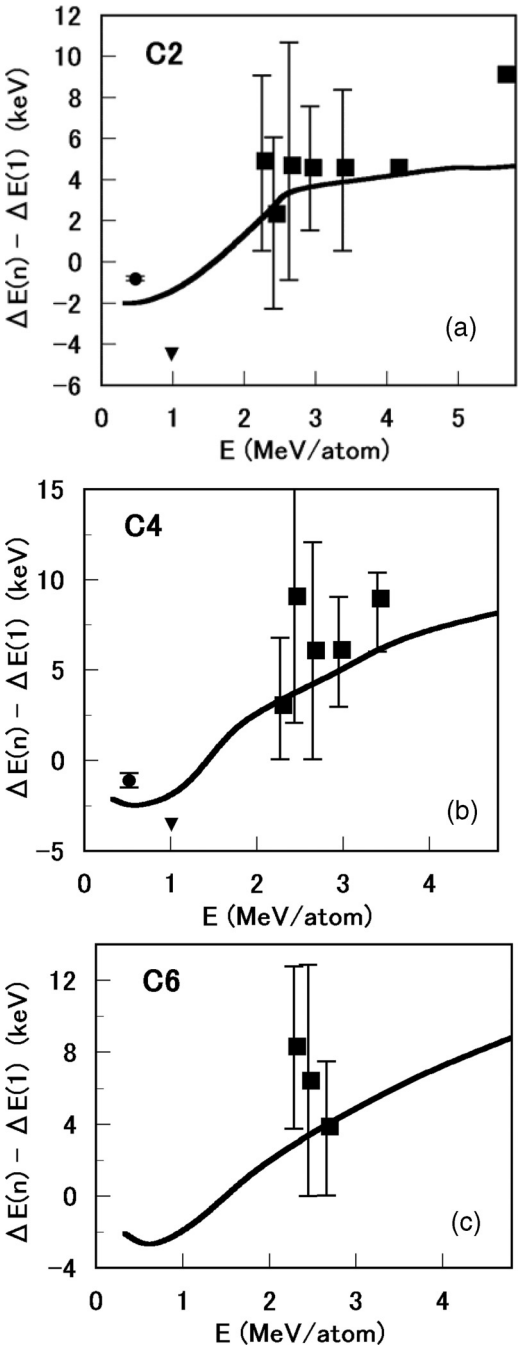

FIG. 10. $\Delta E(n) - \Delta E(1)$ as a function of the incident energy (a) for C_2, (b) for C_4, and (c) for C_6. The experimental data: ■, Baudin *et al.* [21]; ●, Tomita *et al.* [25]; ▼, Brunelle *et al.* [18]. The calculated result: solid lines.

($n = 4$), and the thick solid line ($n = 6$) tend to approach the thin solid line ($n = 1$), as the speed increases. It is noticed that the stronger the binding effect becomes, the more the curve of $Q(n)$ shifts toward the higher-speed side. Figure 10 shows the energy-loss difference, $\Delta E(n) - \Delta E(1)$, for a C_n^+ ($n = 2,4,6$) ion penetrating a carbon foil of $480a_0$ thickness, as a function of the incident energy per atom. Regarding C_2^+ incidence, shown in Fig. 10(a), the value of $\Delta E(n) - \Delta E(1)$ changes around 1.5 MeV/atom from negative to positive; this we call the threshold energy. In addition, it can be seen that

the calculated value of $\Delta E(n) - \Delta E(1)$ increases gradually with increasing incident energy over 2.5 MeV/atom. In the positive region, the calculated result is in good agreement with the experimental data obtained by Baudin *et al.* [21], though those data have large error bars. On the other hand, in the negative region, our result agrees well with the recent data obtained at 0.5 MeV/atom by Tomita *et al.* [25], where they have a small error bar, and the data obtained at 1.01 MeV/atom by Brunelle *et al.* [18]. Figures 10(b) and 10(c) represent $\Delta E(n) - \Delta E(1)$ in the cases of C_4^+ and C_6^+ incidence, respectively. The trends of those calculated result are similar to the case of C_2^+ incidence and the threshold energies are located at almost the same value for C_n^+ ($n = 2,4,6$) incidence. Moreover, comparing the three theoretical curves, we find the remarkable aspect that the increase of $\Delta E(n) - \Delta E(1)$ against the incident energy in the positive region becomes steeper as the particle number increases. The decreasing trend obtained for C_6^+ incidence by Baudin *et al.* [21] with increasing energy cannot be found in the present calculation.

Finally, we give several comments for elaboration. First, the contribution of a small-angle elastic collision to enlargement of the internuclear separation is in substance negligibly small for the swift cluster ions penetrating thin foils investigated here. Consider the case of $E = 0.675$ MeV/atom, which is expected to have a prominent contribution of elastic scattering in this paper. According to the numerical evaluation, we have $\langle\theta^2\rangle_{\text{c.m.}} = 2.2 \times 10^{-4}$, $\sigma = 1.6a_0^2$, $\lambda = 2.0$ nm, $n = 13$, which yields $\Delta_1^2 \simeq 2.2 \times 10^{-4}\,(\text{nm})^2$. Then the enlarged separation is evaluated as $\widetilde{d_{12}} = 0.1289$ nm and $\widetilde{d_{12}}/d_{12} = 1.013$ when the separation without elastic collision is assumed to be $d_{12} = 0.1272$ nm. With increasing incident energy, the mean free path of elastic collision is growing and the scattering probability is strongly diminishing. In an extreme case, the mean free path exceeds the foil thickness. Thus, the elastic collision hardly influences the numerical results presented in this paper. If a larger-angle elastic collision were to occur in a foil, one or more constituent ions in a cluster would be eliminated in one event detection catching all constituent ions after transmission. This case is out of the present consideration. Second, let us give a comment on the energy straggling in a foil. According to the estimate Eq. (18), which includes the contribution of four conduction electrons and two $1s$ electrons per carbon atom, we have $\Omega_C^2/Nx = 1.0 \times 10^{-11}\,\text{eV}^2\,\text{cm}^2$ and $3.46 \times 10^{-11}\,\text{eV}^2\,\text{cm}^2$ for a carbon ion at $E = 675$ keV/atom and 4.8 MeV/atom, respectively. Then, for a carbon ion penetrating a carbon foil of $480a_0$ thickness with $E = 675$ keV/atom and 4.8 MeV/atom, the energy straggling values are $\Omega_C = 1.70$ keV and 3.16 keV, respectively. Although these values bring about the broadening of energy-loss spectra, the θ-dependent energy loss shown in the figures cannot be washed out.

In conclusion, we studied the cluster effect in the average charge and the energy loss for MeV/atom carbon clusters in a linear-chain structure penetrating a carbon foil. Regarding the cluster average charge, the sublinear effect is found regardless of the incident energy. If we increase the incident energy and the number of atoms in a cluster, this negative effect is enhanced as far as the present study is concerned. On the other hand, the energy loss of the carbon-cluster ions incident on carbon foil at the lower energies lower (greater) than the threshold energy ($\sim$1.5 MeV/atom) is found to be weaker (stronger) than the linear dependence on the number of constituent particles. The sublinear and superlinear effects theoretically obtained were in good agreement with the existing experimental data. The sublinear dependence is in contrast to a recent theoretical result [22], predicting superlinear dependence. We remark that the reduction of the cluster average charge plays a significant role in the sublinear dependence of the cluster energy loss. On the other hand, at incident energies greater than the threshold, the present theory was also found to predict the positive cluster effect in nice agreement with the data, though taking into account the sublinear cluster effect in the average charge. We also point out that the postfoil effect enlarges the energy straggling while the average energy loss of the whole cluster is kept unchanged. This effect will be especially magnified under the parallel ($\theta = 0$) incident condition. This new contribution to energy straggling is unique to cluster incidence.

ACKNOWLEDGMENTS

The author thanks Professor H. Kudo and Dr. S. Tomita of the University of Tsukuba and Dr. A. Chiba, Dr. Y. Saitoh, and Dr. K. Narumi of JAEA cluster group, Takasaki, for valuable discussions. The author is grateful to Professor H. Ogawa of Nara Women's University for useful discussion.

[1] P. Attal, S. Della-Negra, D. Gardes, J. D. Larson, Y. Le. Beyec, R. Vienet-Legue, and B. Waast, Nucl. Instrum. Methods Phys. Res., Sect. A **328**, 293 (1993).

[2] I. Yamada, J. Matsuo, N. Toyoda, and A. Kirkpatrick, Mater. Sci. Eng., R **34**, 231 (2001).

[3] B. Farizon, M. Farizon, M. J. Gaillard, E. Gerlic, and S. Ouaskit, Nucl. Instrum. Methods Phys. Res., Sect. B **88**, 86 (1994).

[4] A. Itoh, H. Tsuchida, T. Majima and N. Imanishi, Phys. Rev. A **59**, 4428 (1999); A. Itoh, H. Tsuchida, T. Majima, S. Anada, A. Yogo, and N. Imanishi, *ibid.* **61**, 012702 (1999); H. Tsuchida, A. Itoh, K. Miyabe, Y. Bitoh and N. Imanishi, J. Phys. B **32**, 5289 (1999).

[5] T. LeBrun, H. G. Berry, S. Cheng, R. W. Dunford, H. Esbensen, D. S. Gemmell, E. P. Kanter, and W. Bauer, Phys. Rev. Lett. **72**, 3965 (1994).

[6] A. Faibis, G. Goldring, M. Hass, R. Kaim, I. Plesser and Z. Vager, Nucl. Instrum. Methods **194**, 299 (1982).

[7] K. Wohrer, M. Chabot, J. P. Rozet, D. Gardes, D. Vernhet, D. Jacquet, S. Della Negra, A. Brunelle, M. Nectoux, M. Pautrat, Y. Le. Beyec, P. Attal and G. Maynard, J. Phys. B **29**, L755 (1996); M. Chabot, K. Wohrer, J. P. Rozet, D. Gardes, D. Vernhet, D. Jacquet, S. Della Negra, A. Brunelle, M. Nectoux, M. Pautrat, Y. Le. Beyec, Phys. Scr., T **73**, 282 (1997).

[8] K. Hirata, Y. Saitoh, A. Chiba, M. Adachi, K. Yamada and K. Narumi, Nucl. Instrum. Methods Phys. Res., Sect. B **266**, 2450 (2008); K. Hirata, Y. Saitoh, K. Narumi and Y. Kobayashi, Appl. Phys. Lett. **81**, 3669 (2002).
[9] A. Brunelle, S. Della-Negra, J. Depauw, D. Jacquet, Y. LeBeyec, M. Pautrat, Phys. Rev. A **59**, 4456 (1999).
[10] T. Kaneko, Phys. Rev. A **66**, 052901 (2002).
[11] A. Chiba, Y. Saitoh, K. Narumi, M. Adachi, and T. Kaneko, Phys. Rev. A **76**, 063201 (2007).
[12] H. Kudo, W. Iwazaki, R. Uchiyama, S. Tomita, K. Shima, K. Sasa, S. Ishii, K. Narumi, H. Naramoto, Y. Saitoh, S. Yamamoto and T. Kaneko, Jpn. J. Appl. Phys. **45**, L565 (2006).
[13] S. Tomita, S. Yoda, R. Uchiyama, S. Ishii, K. Sasa, T. Kaneko and H. Kudo, Phys. Rev. A **73**, 060901(R) (2006).
[14] T. Kaneko, H. Kudo, S. Tomita, and R. Uchiyama, J. Phys. Soc. Jpn. **75**, 034717 (2006).
[15] H. Kudo, H. Arai, S. Tomita, S. Ishii and T. Kaneko, Vacuum **84**, 1014 (2010).
[16] M. Vicanek, I. Abril, N. R. Arista, and A. Gras-Marti, Phys. Rev. A **46**, 5745 (1992).
[17] T. Kaneko, Nucl. Instrum. Methods Phys. Res., Sect. B **88**, 86 (1994).
[18] A. Brunelle, S. Della-Negra, J. Depauw, D. Jacquet, Y. Le. Beyec, M. Pautrat, and Ch. Schoppmann, Nucl. Instrum. Methods Phys. Res., Sect. B **125**, 207 (1997).
[19] T. Kaneko, Nucl. Instrum. Methods Phys. Res., Sect. B **153**, 15 (1999).
[20] E. Ray, R. Kirsch, H. H. Mikkelsen, J. C. Poizat, and J. Remillieux, Nucl. Instrum. Methods Phys. Res., Sect. B **69**, 133 (1992).
[21] K. Baudin, A. Brunelle, M. Chabot, S. Della-Negra, J. Depauw, D. Gardes, P. Hakansson, Y. Le. Beyec, A. Billebaud, M. Fallavier, J. Remillieux, J. C. Poizat, and J. P. Thomas, Nucl. Instrum. Methods Phys. Res., Sect. B **94**, 341(1994).
[22] S. Heredia-Avalos, R. Garcia-Molina, and I. Abril, Phys. Rev. A **76**, 012901 (2007).
[23] C. Tomaschko, D. Brandl, R. Kuegler, M. Schurr and H. Voit, Nucl. Instrum. Methods Phys. Res., Sect. B **103**, 407 (1995).
[24] A. Chiba, Y. Saitoh, K. Narumi, Y. Takahashi, K. Yamada and T. Kaneko, Nucl. Instrum. Methods Phys. Res., Sect. B **269**, 824 (2011).
[25] S. Tomita, M. Murakami, N. Sakamoto, S. Ishii, K. Sasa, T. Kaneko, and H. Kudo, Phys. Rev. A **82**, 044901 (2010).
[26] J. Lindhard and A. Winther, Mat. Fys. Medd. K. Dan. Vidensk. Selsk. **34**, 1 (1964).
[27] T. Kaneko, Phys. Rev. A **40**, 2188 (1989); Phys. Status Solidi B **156**, 49 (1989); At. Data Nucl. Data Tables **53**, 271 (1993).
[28] J. Lindhard, V. Nielsen, and M. Scharff, Mat. Fys. Medd. K. Dan. Vidensk. Selsk. **36**, 10 (1968).
[29] P. Sigmund and K. B. Winterbon, Nucl. Instrum. Methods **119**, 541 (1974).
[30] J. F. Ziegler, J. P. Biersack, and U. Littmark, *The Stopping and Range of Ions in Solids* (Pergamon, New York, 1985).
[31] S. Ikegami and T. Kaneko, Bull. Okayama Univ. Sci. A **42**, 21 (2006); T. Kaneko and S. Ikegami, Nucl. Instrum. Methods Phys. Res., Sect. B **258**, 57 (2007).
[32] N. Bohr, Mat. Fys. Medd. K. Dan. Vidensk. Selsk. **18**, 8 (1954).
[33] F. Besenbacher, J. U. Andersen, and E. Bonderup, Nucl. Instrum. Methods **168**, 1 (1980).
[34] T. Kaneko and Y. Yamamura, Phys. Rev. A **33**, 1653 (1986).
[35] M. F. Steuer, D. S. Gemmell, E. P. Kanter, E. A. Johnson, and B. J. Zabransky, Nucl. Instrum. Methods Phys. Res. **194**, 277 (1982).
[36] M. F. Steuer and R. H. Ritchie, Nucl. Instrum. Methods Phys. Res., Sect. B **40-41**, 372 (1989).